Organic Photodiodes Deposited on Newspaper

Organic semiconductors have received significant interest recently and are under serious consideration for use in flexible electronics on a wide variety of substrates. In particular, organic photodiodes have seen rapid improvements in properties and performance. In a recent study, B. Lamprecht and co-workers at Günther Leising's Institute of Nanostructured Material and Photonics in Weiz, Austria, a division of Joanneum Research, have demonstrated the fabrication and characterization of organic photodiodes deposited on ordinary newspaper sheets. They reported their results in the April issue of *Physica Status Solidi A* (p. R50; DOI: 10.1002/pssa.200510010).

The paper samples, taken from the German newspaper *Die Zeit*, were mounted on glass substrates during the fabrication process. The newspaper substrates were coated with a parylene C barrier layer (5–10 μm thick), which is an effective chemical and moisture barrier. Since the newspaper surface is rough, and the parylene coating does not provide a smoothing effect, an ORMOCER coating, which is a new class of silicate-based inorganic–organic hybrid polymer materials, was applied. The ORMOCER coating, ~100 μm thick, provided surface planarization and was inert to subsequent depositions of metal and organic layers. The rms surface roughness at this point was less than 3 nm. The organic charge-generating layers were then deposited, sandwiched between a 55-nm-thick gold bottom electrode and a 25-nm-thick semitransparent silver top electrode. The fabricated organic photodiode, similar to the well-understood Tang-type *pn*-heterojunction device, consisted of a *p*-type conducting copper phthalocyanine (CuPc) and an *n*-type perylene tetracarboxylic bisbenzimidazole. The organic and metal layers were deposited using room-temperature, high-vacuum sublimation. The fabricated devices were removed from the glass substrates prior to characterization.

The current–voltage characteristics of the devices were measured in the dark and under illumination using a halogen lamp, with white light passing through the semitransparent Ag electrode. In the dark, the devices showed a well-pronounced rectification ratio of about 10^4 at ±1 V. On illumination, the devices yielded a photocurrent exceeding the dark current by about six orders of magnitude when operated near a zero bias condition. No hysteresis effect was observed. The photodiodes yielded very good diode behavior. Also, in order to determine the spectral response of the device, measurements of spectrally resolved external quantum efficiency were carried out using a tungsten halogen lamp and a monochromator. The devices yielded a spectral response covering the complete ultraviolet and visible light range. The researchers said that although newspaper was used as an example, from a wider perspective, this study demonstrated that organic photodiode devices may likely be fabricated on almost any user-defined substrate.

GOPAL RAO

Al-Based Tunnel Junctions Form Solid-State Refrigerator Suitable for Sub-Kelvin Applications

Many cutting-edge analytical and astronomical devices require cryogenic operating temperatures of ~100 mK. Current methods for chilling to the 0.1 K range, such as adiabatic demagnetization refrigerators (ADR), can be costly and impractical. As an alternative, A.M. Clark and N.A. Miller of the National Institute of Standards and Technology (NIST), along with co-workers from NIST and the University of Notre Dame, have demonstrated a solid-state refrigerator based on normal metal–insulator–superconductor (NIS) junctions composed of Al and Al-Mn electrodes. The refrigerator has limited cooling capacity, but is suitable for critical applications in which a primary refrigerator or liquid cryogen cools a device to subkelvin temperatures, and the solid-state refrigerator provides a secondary cooling source to pull a device below a critical temperature. As reported in the April 25 issue of *Applied Physics Letters* (173508; DOI 10.1063/1.1914966), the devices can effectively cool large-area Si_3N_4 membranes as well as electrically isolated bulk payloads placed on the membrane.

The NIS refrigerators (see Figure 1) are fabricated using typical thin-film lithography processes, making them easy to integrate with other solid-state devices. The refrigerators are designed with pure Al as the superconductor, Al doped with Mn as the normal metal, and an Al-Mn oxide as the insulator. Four pairs of 25 μm × 15 μm NIS junctions surround a 450 μm × 450 μm Si_3N_4 membrane formed by deep reactive ion etching. Al-Mn cold fingers extend from the refrigerator junctions onto the edges of the suspended membrane, and perforations isolate the fingers and membrane from the substrate. The fingers and membrane are coated with separate Au films to enhance thermal conductivity. Additional NIS junctions (5 μm × 5 μm) were incorporated as temperature sensors. When the refrigerator junctions are under bias, the hottest (highest energy) electrons tunnel from the normal metal fingers away into the superconducting metal. The very low phonon thermal conductance (compared to electron or electron–phonon) allows the entire membrane to be cooled by the cold fingers.

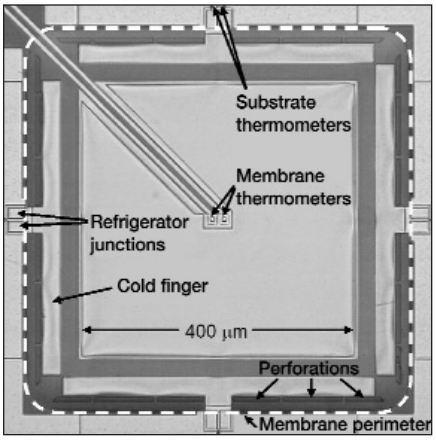

Figure 1. Optical micrograph of metal–insulator–superconductor refrigerator.

The researchers used an ADR to chill the devices for calibration and characterization. At an optimal applied bias of 0.91 Δ/e, where Δ = 189 μeV is the superconducting bandgap energy, the devices were able to reduce the membrane temperature from a starting point of 320 mK to 225 mK and from a starting point of 260 mK to 175 mK. The refrigerators were able to cool a 250 μm cube of doped Ge placed on the membrane from 320 mK to ~240 mK. The cooling power is 40–80 pW, which is sufficient to cool five cryogenic photon sensors without raising the temperature of the cold fingers by more than 5 mK. The researchers are working to further improve performance by better heat-sinking of the superconductor and developing a normal metal with a higher thermal conductivity than the Al-Mn. The researchers also indicated that multistage designs should be easy to fabricate and indicated that a three-stage design should be able to cool objects from an initial temperature of 500 mK to ~10 mK.

AMANDA GIERMANN

Gold Nanoshell Bioconjugates Used for Molecular Imaging in Living Cells

Optical imaging is playing a dramatic role in cancer therapy by aiding early detection, critical to reducing mortality rates. Optical imaging of molecular-specific contrast agents offers real-time *in vivo* monitoring of abnormalities before pathologic changes occur on the atomic level. In the May 1 issue of *Optic Letters* (p. 1012), C. Loo, R. Drezek, N. Halas, and co-workers from Rice University described how

nanoshell bioconjugates can be used to effectively target and image human epidermal growth factor receptor 2 (HER2—a relevant biomarker that is prevalent in human breast carcinoma cells). The researchers chose nanoshells composed of a dielectric silica core surrounded by a thin metallic shell composed of gold whose optical properties can be adjusted by controlling their dimensions. Nanoshells have a strong optical resonance that can be tuned in wavelength across the visible and infrared spectrum, allowing the relative contributions of scattering and absorption at a given wavelength to be tuned by controlling the dimensions of the core and the shell. In this study, nanoshells with a 240-nm-diameter silica core and a 35–nm-thick gold shell were used. By utilizing these nanoshells, it is possible to conjugate bio-relevant materials, in this case, proteins that facilitate *in vivo* imaging.

The researchers attached a linker complex—either anti-HER2 or anti-IgG antibodies–PEG (poly ethylene glycol)—to the nanoshell surface. These conjugated nanoshells where exposed to HER2 expressing SKBr3 cells and studied by dark-field microscopy. A significant increase in optical contrast was observed in the HER2 positive cells targeted with anti-HER2-labeled nanoshells as compared to anti-IgG-labeled nanoshells or cells not exposed to the nanoshell conjugates. The researchers said that nanoshell-based conjugates offer the next generation to *in vivo* imaging due to their near-infrared tunability, size flexibility, and systemic control of optical properties.

LARKEN E. EULISS

Hybrid Photoelectrodes for Solar Water Splitting

Efficient production of hydrogen from water using solar energy is a much-sought-after research goal that has eluded scientists for many years. The wide-bandgap materials that are used in single-junction electrochemical devices to carry out water splitting processes typically absorb sunlight poorly, resulting in low solar-to-hydrogen (STH) conversion efficiencies. Recently, E.L. Miller and colleagues from the Hawaii Natural Energy Institute at the University of Hawaii developed a prototype multijunction photoelectrode proposed to more effectively harness the sun's energy for hydrogen production than has been previously possible.

In the May issue of *Electrochemical and Solid-State Letters* (p. A247), the researchers reported on the performance characteristics of a prototype hybrid photoelectrode (HPE) device and discussed materials developments that will be necessary to improve the STH efficiency. An HPE is a monolithic thin-film device that integrates photoelectrochemical (PEC) and photovoltaic (PV) components in a multiple-junction arrangement. In such a device, the efficiency of hydrogen production is ideally proportional to the photocurrent in the PEC semiconductor, and thus optimum performance is achieved by maximizing this photocurrent.

The prototype HPE described and tested by the research group consists of an *a*-SiGe/*a*-SiGe tandem structure coated with a sputtered WO_3 thin film. This device operated at a hydrogen photocurrent level of 0.5 mA/cm^2 in outdoor sunlight conditions. This corresponds to an STH efficiency of 0.6%. The researchers estimated that peak photocurrents of 0.7 mA/cm^2 could be obtained from this device.

Although the results are promising, these materials clearly do not offer optimal device performance; novel materials must be developed for use as the PEC and PV components. One upgrade suggested by the researchers is the use of "improved" sputtered WO_3 coatings. These films offer peak photocurrents of 2.4 mA/cm^2, which represent a threefold increase in peak photocurrent and ideally a corresponding improvement in STH. The researchers predict that when integrated with a newly developed *a*-Si/*a*-Si tandem structure, an HPE with this improved coating layer would yield STH efficiencies exceeding 2.2%.

The chief limitation of HPE structures at the moment is the maximum photocurrent allowed by the top PEC semiconductor films. Doped TiO_2 or WO_3 films may offer a solution; these feature photocurrent values as high as 5 mA/cm^2. The researchers also suggest that appropriate combinations of PEC and PV materials may yield STH values in excess of 10%. Clearly, much development is necessary to attain such efficient hydrogen production in HPE devices, but these prototype results point to possible significant improvements in efficiency.

ANDY FRANCIS

Distribution of Nanoparticles in Photopolymer Controlled Holographically

Applications for holograms include three-dimensional displays, data storage, and photonics. In recent years, holographic gratings have been fabricated from two-component mixtures of organic photopolymers and from polymer-dispersed liquid crystals. The incorporation of materials that extend the range of the refraction index profile will result in more efficient holograms. For example, a system composed of organic photopolymers and inorganic nanoparticles, which, unlike organic compounds, display a wide range of refractive indices (n), were recently proposed by researchers from the Department of Electronics Engineering, University of Electro-Communications (UEC), Tokyo, although heretofore, the formation mechanism of such holographic gratings was not clearly understood.

As reported in the April 15 issue of *Optics Letters*, UEC researchers Y. Tomita and N. Suzuki and K. Chikama from Chemical Research Laboratories, Nissan Chemical Industries, demonstrated holographic control of morphology in nanoparticle-dispersed photopolymers and explained the formation of the holographic gratings in relatively simple terms of the chemical potential (μ) of non-interacting particles. The researchers combined either SiO_2 nanoparticles (n = 1.46, diameter = 13 nm) or TiO_2 nanoparticles (n = 2.55, diameter = 15 nm) at a volume fraction of 0.34 with methacrylate monomers (n = 1.55 in the liquid and 1.59 in the solid phase at a wavelength of 589 nm) and the initiator titanocene to cast films ~50 μm thick. Transmission-type holograms were then recorded at a grating spacing of 1 μm by exposing the films to two mutually coherent beams at a wavelength of 532 nm. The researchers used transmission electron microscopy to show that the nanoparticles followed the intensity interference fringe pattern at a grating spacing of 1 μm.

Tomita and his colleagues hypothesized a mutual diffusion model in which monomers polymerize in the bright regions, where their μ decreases, leading to the diffusion of monomers from dark to bright regions. The photoinsensitive inorganic nanoparticles, on the other hand, are not consumed during polymerization, and their μ increases in the bright regions, causing them to diffuse to the dark regions. The researchers reasoned that the phase shift (ϕ) between the intensity interference fringe pattern and the recorded holograms should be 0° for the SiO_2 hologram, that is, the change in n (Δn) is highest in the bright regions, because n for SiO_2 is less than n for the polymer. Similarly, ϕ for the TiO_2 hologram should be 180°, that is, Δn is highest in the dark regions, because n for TiO_2 is greater than n for the polymer. Both of these predictions were confirmed by the researchers.

Tomita and his colleagues said that their finding of all-optical control of nanoparticle distribution in photopolymers will facilitate the addition of new functionality to holographic applications, such as the fabrication of nonlinear periodic structures and nonlinear photonic

crystals, through the incorporation of nonlinear optical nanoparticles. Other possibilities mentioned by the researchers include holograms with magnetic nanocrystals for magneto-optic applications and the incorporation of inorganic nanocrystals for multifunctional light-emitting devices.

STEVEN TROHALAKI

Sequential Synthesis of Colloidal Type-II Core/Shell CdTe/CdSe Semiconductor Nanocrystals Demonstrated

Semiconductor nanocrystals have been the subject of recent scientific and technological interest due to their promising potential applications, including photovoltaics and bio-imaging. In heterostructured nanocrystals, a higher-bandgap shell material can be grown onto a core material with a lower bandgap. Type II core–shell nanocrystals are materials engineered by their band offset (ΔE_v), and in these structures, the band offsets are such that the energies of the conduction and valence bands of the shell are either both higher or both lower than those of the core. These materials can spatially separate and confine photo-generated holes and electrons. A common-cation system, CdTe (core)/CdSe (shell) nanocrystals are type II materials, with the majority of photogenerated holes confined in the CdTe core and the electrons in the CdSe shell. Recently, K. Yu and co-workers from the National Research Council of Canada have developed an efficient approach to the synthesis of high-quality CdTe/CdSe nanocrystals. For the CdSe shell, by control of various factors, the technique avoids the formation of a thicker CdSe nanocrystal layer resulting in a thinner shell, leading to a higher photoluminescence efficiency. The researchers report their results in the March issue of *Small*.

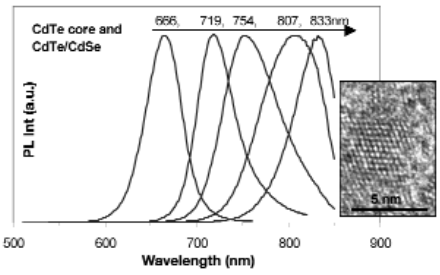

Figure 1. Photoemission spectra of CdTe(core)/ CdSe(shell) nanocrystals showing that the thicker the CdSe shell is, the more the emission redshifts. The inset is a transmission electron micrograph of one core–shell nanocrystal in an ensemble exhibiting 833 nm emission.

Colloidal type II CdTe/CdSe nanocrystals were synthesized by the sequential addition of a tri-*n*-octylphosphine telluride (TOPTe)/tri-*n*-octylphosphine (TOP) solution and several shell-precursor solutions to a cadmium oxide (CdO)/TOP solution. The shell-precursor solutions consist of CdO and tri-*n*-octylphosphine selenide (TOPSe) in TOP. This synthetic approach is simple and does not involve either the addition of any acids, amines, or traditional tri-*n*-octylphosphine oxide (TOPO), or precipitation of core CdTe nanocrystals.

During the synthesis of the type-II CdTe/CdSe nanocrystals, the researchers monitored the temporal evolution of the optical properties during the growth of the CdSe shell, as shown in the figure. The emission redshifts with increasing CdSe shell thickness.

This synthetic approach, similar to that of sequential anionic polymerization for well-defined block copolymers, is based on the knowledge gained during the search for synthetic routes for providing slow growth rates for high-quality CdSe and CdTe nanocrystals in large-scale production. It has been acknowledged that a slower particle growth rate results in less surface roughness, fewer surface defects, and higher photoluminescent efficiency. This synthetic approach is particularly well suited for realizing engineering materials with bandgaps in the near-infrared and infrared spectral ranges.

GOPAL RAO

Far-Field Technique for Visualization of Broadband Surface Plasmons Developed

Surface plasmons (SPs) are traveling waves that propagate along the interface of a metal and an insulator. Commercially available sensors for environmental and biological applications have been fabricated by tailoring the interaction between impinging light and SPs. Recently, SPs have been explored as a means of realizing metallic photonic circuits. Imaging the SP intensity distribution is essential to characterizing SP-based devices. Traditionally, this imaging has been accomplished by near-field and fluorescence techniques. As reported in the April 15 issue of *Optics Letters* (p. 884), A. Bouhelier and G.P. Wiederrecht of the Chemistry Division and Center for Nanoscale Materials at Argonne National Laboratory have developed a far-field method for exciting and observing the SP intensity distribution. The SP intensity distribution was imaged by detecting leakage radiation, which are two of the four electromagnetic modes that are solutions to the dispersion relations.

The researchers deposited silver films onto glass substrates using thermal evaporation. To avoid total internal reflection of the radiative modes, an index-matched, oil-immersed objective (numerical aperture of 1.4) was kept in contact with the glass substrate. The objective was part of an optical microscope, which was focused on the metal–glass interface. White light was used to excite a broadband surface plasmon continuum at the interface. This is possible because the objective introduced a distribution of wave vectors, through focusing, that fulfill the dispersion relation of the plasmon over the entire visible spectral region. The surface plasmon leakage radiation was recorded by a CCD camera that was placed in the image plane. A regeneratively amplified Ti:sapphire laser system was used to produce the incident white-light continuum radiation, which was polarized by a multi-wavelength wave plate and a Glan-Thompson polarizer.

Propagating SPs were visualized by recording the real-space distribution of leakage radiation emitted by SP waves at the dielectric–metal interfaces. The images reveal a spatial variation in the spectral components of the SPs, which the researchers have termed "rainbow jets," that extend a significant distance along the direction of propagation of the SPs away from the incident continuum radiation spot. According to Bouhelier and Wiederrecht, the observation of surface plasmon leakage radiation gives a direct measurement of the SP propagation length and the damping mechanisms for each wavelength. The study of surface plasmons and light–SP interactions opens possibilities for photonics because they allow the concentration and propagation of light below the usual resolution limit, which may enable the realization of wavelength-sensitive optical devices.

JEREMIAH T. ABIADE

Combination of Raman Scattering Techniques Achieve Single-Molecule Detection of Biomolecules

As molecular biology advances, the detection of low quantities of biomolecules is proving critical for some applications, said researchers T.-W. Koo, S. Chan, and A.A. Berlin of the Precision Biology group at Intel Corporation in their article published in the May 1 issue of *Optics Letters* (p. 1024).

Surface-enhanced Raman scattering (SERS), which has been demonstrated as a single-molecule detection method, benefits from signal increases on the order of 10^3–10^{15} primarily because of the electro-

magnetic field enhancements associated with surface plasmon resonances over the non-enhanced Raman scattering methods. However, SERS requires the target molecule to adsorb onto a metal surface to benefit from surface plasmon resonance. Consequently, it has been difficult to detect biological molecules that have a low affinity for metal surfaces, and only a few types of molecules have been detected by SERS with single-molecule sensitivity to date. The researchers said that huge signal gain can be obtained by combining SERS and coherent anti-Stokes Raman scattering (CARS) as is done in surface-enhanced coherent anti-Stokes Raman scattering (SECARS). The researchers further improved the sensitivity of SECARS over the earlier reported work, and achieved single-molecule detection of some biomolecules not detected earlier using this method.

The researchers said that SECARS background originating from metal and water has limited the sensitivity of previous works. The research group used several methods, such as a polarization-sensitive CARS setup, minimized probe volume, and the use of aggregated colloidal silver nanoparticles instead of planar substrates, to reduce the background. The SECARS signals of biological molecules were increased by the addition of lithium chloride salts, which were found to be optimal for generating strong surface enhancements.

The researchers then demonstrated the power of SECARS by detecting two DNA nucleotides, deoxyadenosine monophosphate (dAMP) and deoxyguanosine monophosphate (dGMP), and a peptide—angiotensin-I peptide. Although dAMP has been detected at the single-molecule level by SERS, the SECARS signal was approximately 1000 times stronger than the SERS signal for dAMP at single-molecule concentrations. The SECARS signal of dGMP was at least 100 times stronger than the SERS signal of dGMP. The researchers believe that this is the first reported detection of dGMP at single-molecule concentrations.

The detection of the peptide shows that the SECARS technique can be applied to biological molecules other than nucleotides. According to the research group, the ultrasensitive detection of nonlabeled peptides and proteins has potential applications in pathogen detection, disease monitoring, and drug discovery.

VIVEK RANJAN

Cell Membranes Integrated into CNT Devices

Integrating biological systems and processes with nanofabricated structures is a critical challenge for nanotechnology. In the May issue of *Nano Letters*, J.-C. Gabriel, G. Grüner, and their co-workers reported on their work, performed at Nanomix Inc., on the integration of the cell membrane of *Halobacterium salinarum* with carbon nanotube (CNT) network transistors, wherein both the biological and nanoelectronic structures preserve their functionality and are able to electronically interact with each other.

The researchers fabricated nanotube network field-effect transistors, where the semiconducting channel is formed by a network of predominantly semiconducting nanotubes. A monolayer of the purple membrane from *Halobacterium salinarum* was then deposited on the exposed semiconductor channel. Evidence for the integration of the membrane with the device comes from changes in the device characteristics of the transistor.

The purple membrane contains bacteriorhodopsin, which has a permanent electric dipole moment pointing from the extracellular side of the membrane toward the cytoplasmic side. The researchers prepared three sets of devices. The first had the membrane dipole randomly oriented on the nanotubes, while the second and third sets had the cytoplasmic or extracellular side of the membrane facing the nanotubes. Prior to integration of the membrane, the nanotube devices by themselves worked as *p*-type transistors with good conduction at negative gate voltages and no conduction at positive gate voltages. The voltage at which the device turns on is known as the threshold voltage and is different depending on the sweep direction of the gate voltage (i.e., it is hysteretic). The hysteresis is known to be produced by water adsorbed on the substrate.

For the mixed-orientation nanobioelectronic device, deposition of the cell membrane resulted in a narrower hysteresis compared with the hysteresis of the nanotube devices alone. The researchers attributed this effect to desorption of water from the nanotube surface as the membrane displaced water. Also, the turn on for this device was less sharp, indicating a change in carrier mobility for the nanotube networks arising from random scattering potentials due to the electric dipoles of rhodopsin. The oriented membrane devices also showed a loss of hysteresis and a shift of the threshold voltage in different directions for the two different orientations of the membrane. Since the threshold voltage is correlated to the position of the Fermi level in nanotubes, the shift in the threshold voltage is indicative of a charge induced in the nanotube by the electric dipole of the membrane. The magnitudes of the shifts are different for the two orientations, implying asymmetry in the charge distribution of rhodopsin, with the dipole being closer to the cytoplasmic side.

Grüner, who is a professor at UCLA and advisor to the project, said that this work "opens up avenues for what could be called 'cellectronics,' the electronic detection and also modification of biological processes at the cellular level."

SARBAJIT BANERJEE

Continuous-Wave 1.94 µm Laser Based on Tm:BaY_2F_8 Lases from 1849 nm to 2059 nm

Efficient, widely tunable solid-state laser sources in the near-infrared region around 2 µm have potential applications in remote sensing and gas detection, high-resolution spectroscopy, frequency metrology, and medicine. Thulium doping of crystals can be used in this wavelength region because of the $^3F_4$–$^3H_6$ optical transition of Tm^{3+} ions that in most host media yields a very broad emission with a maximum at wavelengths of ~1.8–1.9 µm. In addition, Tm^{3+} has the advantage that it can be directly diode-pumped at ~785 nm, and shows a quantum efficiency close to 2 (i.e., each pump quantum absorbed yields two Tm ions in the upper laser level).

In the April 15 issue of *Optics Letters* (p. 854), G. Galzerano and P. Laporta of Politecnico di Milano, in a joint collaboration with M. Tonelli and colleagues from the Università di Pisa, Italy, described the growth, spectroscopic characterization, and laser action of a diode-pumped laser based on a Tm-doped fluoride crystal (Tm:BaY_2F_8). They reported a room-temperature, diode-pumped laser oscillator widely tunable over a 210 nm interval, from 1849 nm to 2059 nm, with a maximum continuous-wave (cw) output power of ~150 mW at 1920 nm by use of a 0.5% output coupler transmission.

The researchers said that fluoride crystals, despite thermomechanical properties that are usually poorer than those of most oxides, present some advantages in terms of laser performance. These include low phonon energy, longer fluorescence lifetime, lower upconversion losses, reduced thermal lensing, and extremely low-beam depolarization under strong pumping. The crystal was grown in a homemade Czochralski furnace, starting with BaY_2F_8 powder and adding BaF_2 and TmF_2 powders. The best laser results were obtained for a Tm doping level of 12%. Crystallinity and crystallographic orientation were determined from x-ray

Laue results, which enabled the preparation of oriented samples.

The laser resonator was a three-mirror folded cavity configuration to allow compensation of a slight astigmatism introduced by the laser crystal. The 2.2-mm-long laser crystal was placed at a Brewster's angle close to the plane high-reflectivity mirror and was mounted on a copper heat sink without any cooling system. The Tm:BaY_2F_8 was longitudinally pumped by a GaAlAs laser diode at a wavelength of ~780 nm with a maximum cw output power of 3 W. Tuning of the laser wavelength was accomplished by adjustment of an intracavity quartz plate acting as a birefringent filter. The free-running laser showed cw oscillation over a wide range of wavelengths that depended on the specific configuration. Increasing the output coupling increased the output power, but decreased the wavelength tuning range. The lower-wavelength end of the tuning range (i.e., 1850 nm) was limited by the bandwidth of the dielectric laser mirrors that were used. The wavelength-shift of up to 2059 nm, compared with the longest emission wavelength observed in the fluorescence spectrum, at 1925 nm, is ascribed to the vibronic behavior of the laser crystal. To the researchers' knowledge, this is the largest shift ever observed for a rare-earth laser.

ROSALÍA SERNA

Nanotube Coupled with Nanodiamond Forms Hybrid Nanomaterial

The increasing scale of device integration in solid-state technology, coinciding with decreasing structure dimensions, requires the use of nanomaterials that can be engineered to form nanoscale architectures, built from units with desired shapes and properties. Moreover, such materials must survive under severe conditions. In this context, the family of carbon nanostructures is ideally suited for a wide range of innovative applications, and their chemical compatibility makes hybrid nanomaterials that couple nanotubes and nanodiamond an attractive prospect. Recently, M.L. Terranova and colleagues of the University of Rome "Tor Vergata," M. Rossi of the University of Rome "La Sapienza," and A.S. Barnard of Argonne National Laboratory have produced ordered deposits of tubular nanostructured carbon that couple diamond nanocrystals with single-walled carbon nanotubes.

In a forthcoming issue of *Chemistry of Materials* (DOI: 10.1021/cm0502018), Terranova, Rossi, and colleagues outlined a systematic method for the growth of these hybrid nanocarbons, involving the reaction of graphitic carbon nanopowders (produced by cw-laser-assisted pyrolysis of hydrocarbon mixtures) with atomic H, in a modified chemical vapor deposition reactor. The carbon nanopowders were carried from a reservoir by Ar streams and homogeneously delivered across the active area of a Si substrate coated by a submicron dispersion of Fe particles. The experimental parameters were outlined, and it was shown that under well-defined conditions, the production of ordered arrays of rigid nanotubes coated by diamond nanocrystals was possible during the same run. The final deposits consisted of vertically aligned, tubular bundles of single-walled carbon nanotubes up to 15 μm long, coated with an outer deposit of well-shaped diamond nanocrystals (see Figure 1), attached to the nanotubes by a reduced portion of their base. To facilitate the investigation of the formation of these materials, the researchers constructed a time–growth sequence by ad hoc experiments performed by changing the duration of the synthesis process in the range of 1–15 min. The samples for each deposition time were characterized, and the growth and evolution of each of the respective nanocarbon phases were confirmed.

The researchers proposed that following nanotube growth, the high relative concentration of atomic H used in the experiments was instrumental in disrupting locally the C–C sp^2 network of the nanotube walls, thereby creating localized C–C sp^3 defects that act as suitable sites for the nucleation of diamond nanocrystals. As soon as the first diamond crystallites were formed, further top-growth of the nanotube was repressed, since further buildup of nanotubes was limited by the initial coverage of diamond nanocrystals. Following crystallization, the nanodiamond growth continued, taking advantage of the surface supersaturation and localized carbon segregation produced by the etching of some of the nanotubes as well as that of the feeding C nanopowders. The final coating of diamond nanocrystals remained as "hanging objects," due to the curvature of the (nanotube) substrate, with typical sizes ranging from 20 nm near the base of the nanotubes to 100 nm at the top.

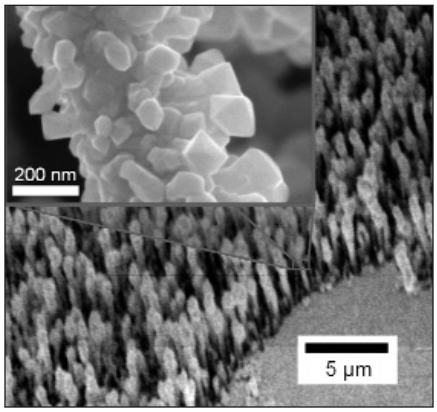

Figure 1. Vertically aligned, tubular bundles of single-walled carbon nanotubes up to 15 μm long, coated with an outer deposit of 20–100 nm of nanodiamond, along with a detailed image (inset) showing the faceted shape of the diamond nanocrystals.

Considering that diamond is one of the most promising wide-bandgap semiconductors for various electronic devices, with an excellent potential due to its negative electron affinity, the researchers said that these rigid rods may find applications as micro- and nanoscale cold-cathode devices, miniaturized cathode-ray tubes, light-emitting displays, micromechanics, and nanoscale sensing.

For more research news on Materials Science, access the Materials Research Society Web site:
www.mrs.org/connections